



RESEARCH ARTICLE

10.1029/2018JA025477

Seasonal and Solar Cycle Variations of Thermally Excited 630.0 nm Emissions in the Polar Ionosphere

Key Points:

- Thermal emissions maximize during equinox and solar maximum
- Thermal emissions are dominated by high electron temperatures at solar minimum and by high electron densities at solar maximum
- There is an equinoctial asymmetry in the occurrence of thermal emissions at Svalbard, which reverses with the solar cycle

Correspondence to:

N. K. Kwagala,
norah.kwagala@uib.no

Citation:

Kwagala, N. K., Oksavik, K., Lorentzen, D. A., Johnsen, M. G., & Laundal, K. M. (2018). Seasonal and solar cycle variations of thermally excited 630.0 nm emissions in the polar ionosphere. *Journal of Geophysical Research: Space Physics*, 123, 7029–7039. <https://doi.org/10.1029/2018JA025477>

Received 14 MAR 2018

Accepted 2 AUG 2018

Accepted article online 9 AUG 2018

Published online 28 AUG 2018

Norah Kaggwa Kwagala^{1,2} , Kjellmar Oksavik^{1,2,3} , Dag A. Lorentzen² , Magnar G. Johnsen⁴, and Karl M. Laundal¹

¹Birkeland Centre for Space Science, University of Bergen, Bergen, Norway, ²Birkeland Centre for Space Science, The University Centre in Svalbard, Longyearbyen, Norway, ³Center for Space Science and Engineering Research (Space@VT), Virginia Polytechnic Institute and State University, Blacksburg, VA, USA, ⁴Tromsø Geophysical Observatory, UiT - The Arctic University of Norway,

Abstract Solar cycle and seasonal variations have been found in the occurrence of strong thermally excited 630.0 nm emissions in the polar ionosphere. Measurements from the European Incoherent Scatter Svalbard Radar have been used to derive the thermal emission intensity. Thermally excited emissions have been found to maximize at solar maximum with peak occurrence rate of ~40% compared to ~2% at solar minimum. These emissions also have the highest occurrence in equinox and the lowest occurrence rate in summer and winter. There is an equinoctial asymmetry in the occurrence rate which reverses with the solar cycle. This equinoctial asymmetry is attributed to variations of the solar wind-magnetosphere coupling arising from the Russell-McPherron effect. The occurrence rate of thermal excitation emission on the dayside, at Svalbard, has been found to be higher in autumn than spring at solar maximum and the reverse at solar minimum. Enhanced electron temperatures characterize the strong thermal component for solar minimum and winter, whereas enhanced electron densities characterize the thermal component for solar maximum. The results point to solar wind-magnetosphere-ionosphere coupling as the dominant controlling process.

1. Introduction

Thermally excited 630.0 nm emissions in the polar ionosphere arise when the ambient ionospheric electrons are rapidly heated by precipitating soft electrons and cooled via excitation of atomic oxygen to the 1-D state, which then de-excites via emission of the 630.0 nm line (Carlson, 1996; Carlson et al., 2013; Johnsen et al., 2012; Kozyra et al., 1990; Kwagala et al., 2017, 2018; Lockwood et al., 1993). Kwagala et al. (2017) found that thermally excited emissions can contribute more than 50% of the observed 630.0 nm emission intensity in the cusp ionosphere. On the basis of existing knowledge, we have done a series of statistical studies of thermally excited 630.0 nm emissions in the polar ionosphere. The first study in the series (Kwagala et al., 2018) presented a general statistical study on occurrence of thermally excited emissions with specific focus on the strong thermal component (intensity >1 kR). They showed that thermally excited emissions mainly occur on the dayside and maximizes around magnetic noon. Earlier literature (e.g., Kozyra et al., 1990; Lockwood et al., 1993) reports 3000 K as the electron temperature beyond which thermally excited emissions can become important. Kwagala et al. (2018) found an additional population of thermally excited emissions at lower temperatures (~2300–3000 K) when extreme electron densities (> 5 × 10¹¹ m⁻³) prevailed.

Little is known about the occurrence of thermally excited emissions in the different seasons. Optical observation of these emissions is not possible when the sun is above the horizon, like during summer at Svalbard. Most cases in literature have been from winter (e.g., Carlson et al., 2013; Kwagala et al., 2017). However, several statistical studies on other aspect like geomagnetic activity have reported seasonal and semiannual variations (e.g., Cliver et al., 2000; Zhao & Zong, 2012). Such variations have been attributed to the variations in the orientation of the Earth's dipole axis with respect to the Parker spiral field, also known as the Russell-McPherron (R-M) effect (e.g., Russell & McPherron, 1973; Zhao & Zong, 2012). In some statistical studies at high latitudes (e.g., Aruliah et al., 1996, 1997, and references therein), the R-M effect has been given as the source of equinoctial asymmetry observed at high latitudes. It is not yet known if such variations will be seen for thermally excited emissions.

©2018. The Authors.

This is an open access article under the terms of the Creative Commons Attribution-NonCommercial-NoDerivs License, which permits use and distribution in any medium, provided the original work is properly cited, the use is non-commercial and no modifications or adaptations are made.

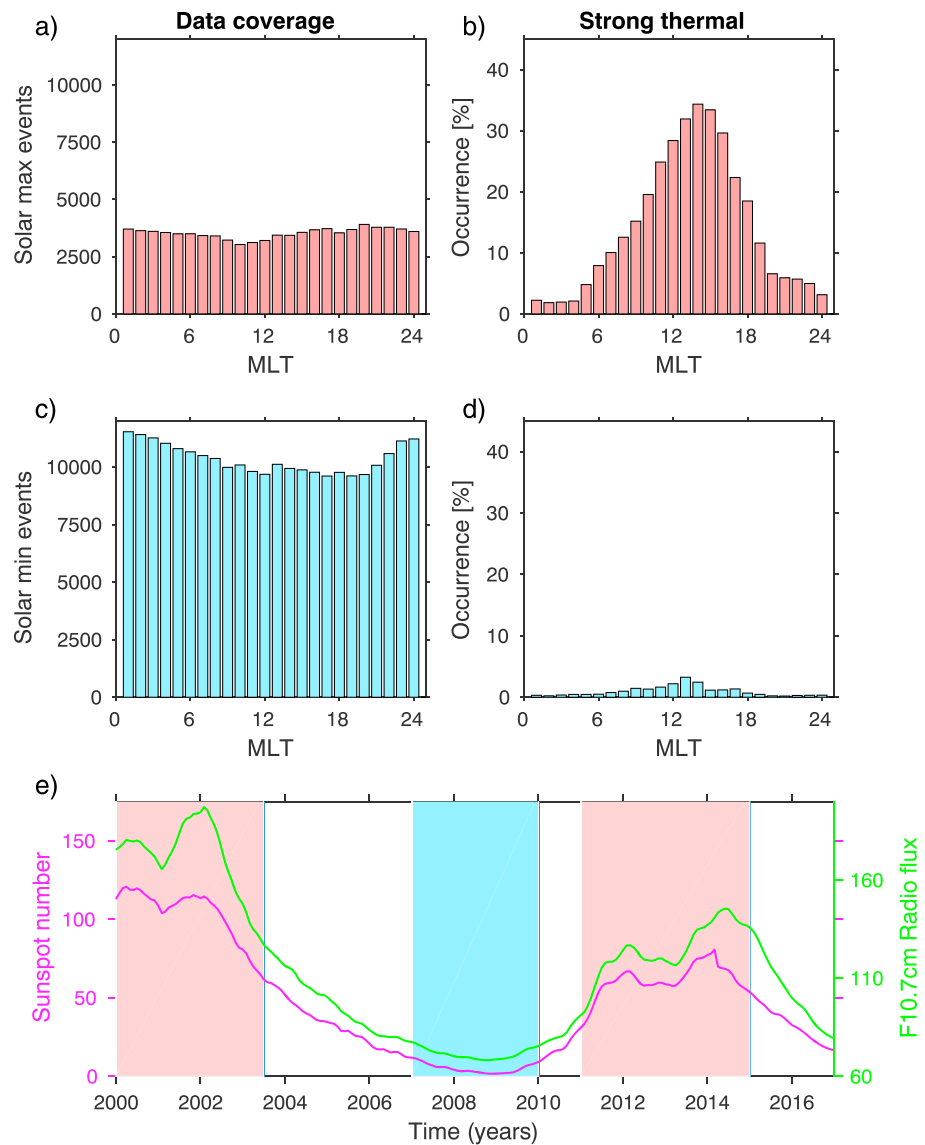


Figure 1. Data coverage for solar maximum (a,b) and solar minimum (c,d). The left column (a,c) is data coverage for reference only, and the right column (b,d) is the MLT distribution of the strong thermal emissions which is the focus of this paper. Panel (e) shows the monthly averaged sunspot number (magenta) and F10.7 cm solar flux (green) progression after year 2000. The red shading is used to indicate the period for solar maximum shown in (a) and (b). The blue shading is used to indicate the period for solar minimum shown in (c) and (d). Higher occurrence rate is seen for solar maximum. MLT = magnetic local time.

In this paper, we therefore investigate seasonal and solar cycle variations of thermally excited emissions. This is the second paper in the series after Kwagala et al. (2018). European Incoherent Scatter (EISCAT) Svalbard Radar (ESR) measurements are used to derive the thermal excitation component. The ESR takes measurements of ionospheric parameters irrespective of cloud cover and/or sunlight conditions. We describe our approach in section 2. Section 3 contains the observations and results. The discussion of results is given in section 4 and our conclusions are summarized in section 5.

2. Approach

In this study, we estimate the thermally excited emission intensity in the polar ionosphere using ESR measurements of electron temperature and density. The data used and methodology are described in this section.

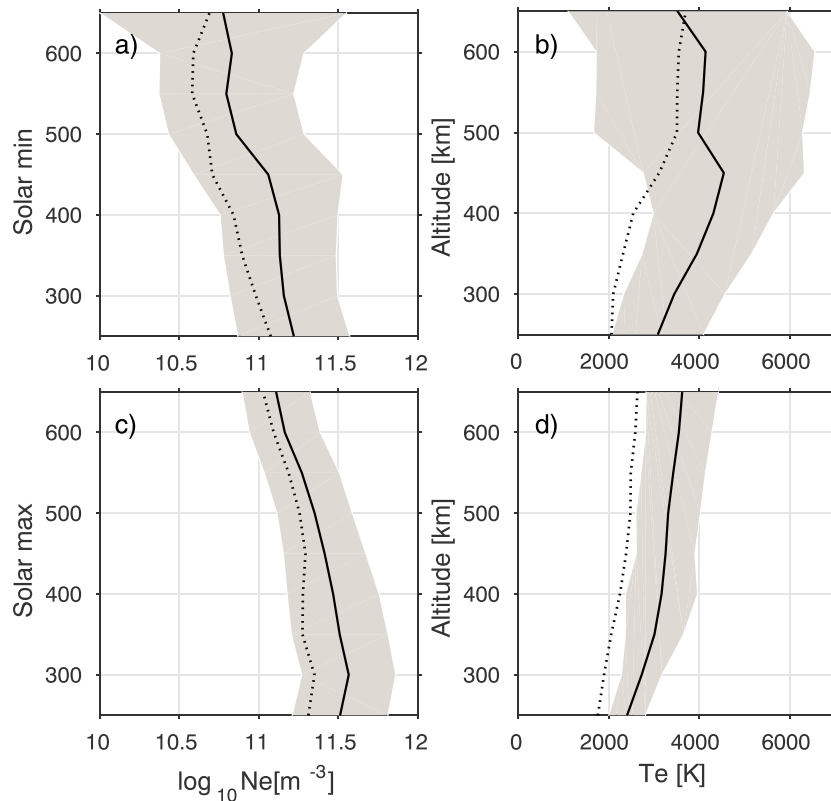


Figure 2. Distribution of electron temperature (b,d) and electron density (a,c) for solar minimum (a,b) and solar maximum (c,d), associated with the strong thermal component. The black line shows the strong thermal average with the gray shading marking the standard deviation of the strong thermal distribution. The dotted line shows the solar minimum/maximum mean for reference.

2.1. Data

Data from the fixed field-aligned ESR 42 m beam for the period 2000–2015 has been used to obtain height profiles for the electron density and electron temperature. The elevation of the 42 m beam is 81.6° from the southern horizon. The difference between the range (line-of-sight) and the height/altitude is 1–3 km. We therefore assume it is close to vertical. ESR is located at 75.12°N quasi-dipole magnetic latitude and magnetic local time is ~UT+3 (geographic coordinates: 78.15°N, 16.02°E). The magnetic local time (MLT) is defined with respect to the subsolar point using Equation 93 of Laundal and Richmond (2017). A description of the ESR is given by Wannberg et al. (1997). The handling of the ESR data for the period of interest in this paper is exactly the same way as compared to Kwagala et al. (2018) and is described in detail therein and is quickly summarized here. The Naval Research Laboratory Mass Spectrometer and Incoherent Scatter Radar 2000 model (NRLMSISE-00; Picone et al., 2002) has been used to generate the number density of atomic oxygen. Also in section 4 we use atomic oxygen density generated by the Thermosphere-Ionosphere-Electrodynamics General Circulation Model (TIE-GCM; Dickinson et al., 1981; Qian et al., 2009, 2014; Richmond, 1995; Roble et al., 1977, 1982) for comparison. The TIE-GCM is a first principles physics-based and self consistent 3-D thermosphere ionosphere model (Qian et al., 2014; Richmond et al., 1992; Roble et al., 1988). The sunspot number and F10.7 cm radio flux is obtained from the NOAA/SWPC database (<ftp://ftp.swpc.noaa.gov/pub/weekly>).

2.2. Method

The volume emission rate is calculated using a formulae provided by Carlson et al. (2013):

$$I_{630}(h) = \alpha [T_e(h)] \times N_o(h) \times N_e(h) \quad (\text{Rayleighs}/\text{km}), \quad (1)$$

and total vertical column intensity is the line-of-sight integration of the volume emission rate:

$$I_{630} = \int_{250\text{km}}^{650\text{km}} I_{630}(h)dh \quad (\text{Rayleighs}), \quad (2)$$

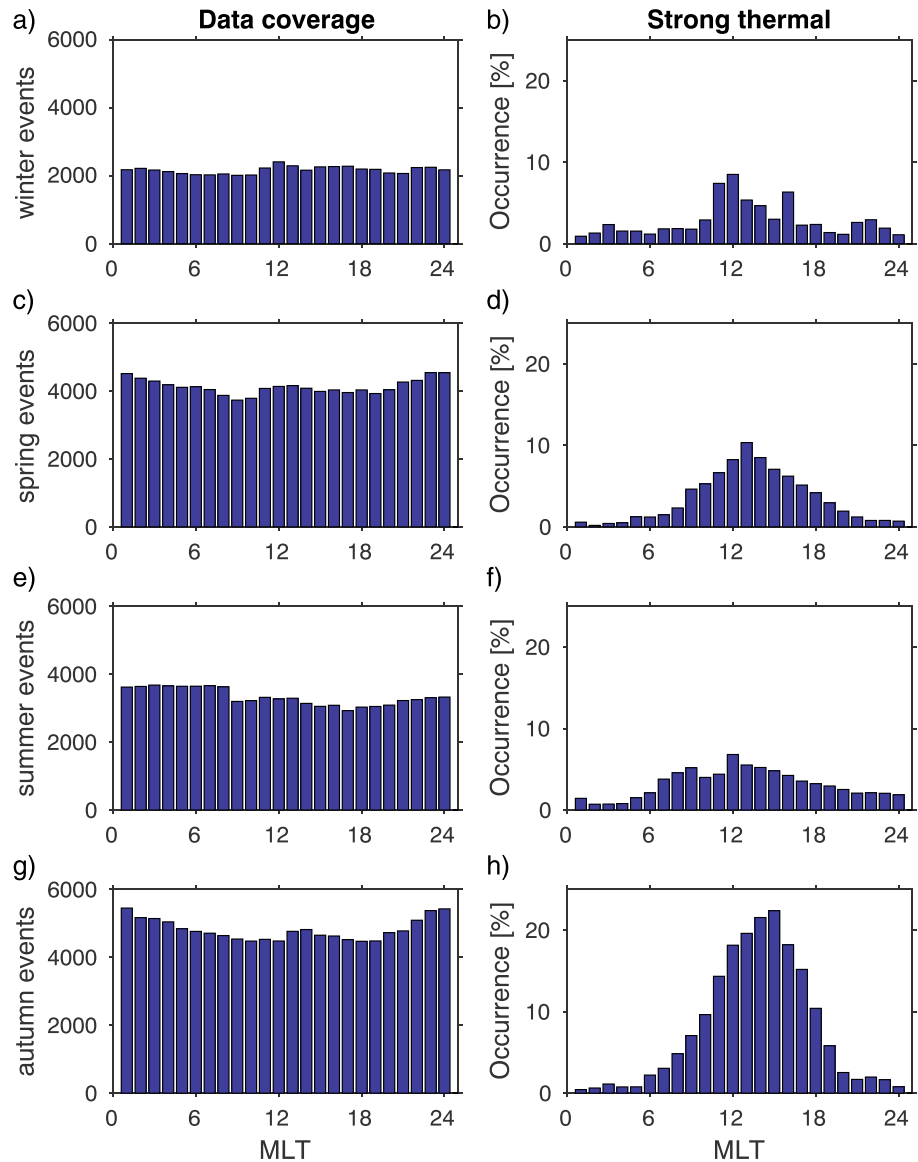


Figure 3. Data coverage for the four seasons of the year: winter (a,b), spring (c,d), summer (e,f), and autumn (g,h). The left column (a,c,e,g) is data coverage for reference only, and the right column is MLT distribution of the strong thermal events that is the focus of this paper. The highest occurrence is seen in equinox (spring and autumn). MLT = magnetic local time.

where

$$\alpha(T_e) = 0.15 \times \sqrt{T_e} \times \frac{(8537 + T_e)}{(34191 + T_e)^3} \times e^{\left(\frac{-22756}{T_e}\right)} \quad (\text{cm}^3/\text{s}) \quad (3)$$

is given by Mantas and Carlson (1991) based on O(¹D) electron impact excitation cross section by Lan et al. (1972) for deriving O(¹D) excitation rates by thermal electron impact. The cross section by Lan et al. (1972) was recommended by Mantas and Carlson (1991) after a reassessment of different values of cross sections provided in literature (e.g., Doering & Gulcicek, 1989; Henry et al., 1969; Lan et al., 1972; Thomas & Nesbet, 1975). T_e is the electron temperature in Kelvins, N_e is the electron density in cm^{-3} , and N_o is the atomic oxygen density in cm^{-3} . All the parameters are functions of altitude h in kilometers. The O(¹D) is, however, susceptible to quenching, mainly by molecular nitrogen. The quenching is frequent at low altitudes (<250 km) where molecular nitrogen dominates. Our study focusses at altitudes above 250 km where the molecular nitrogen density is greatly reduced and we therefore consider quenching to be negligible.

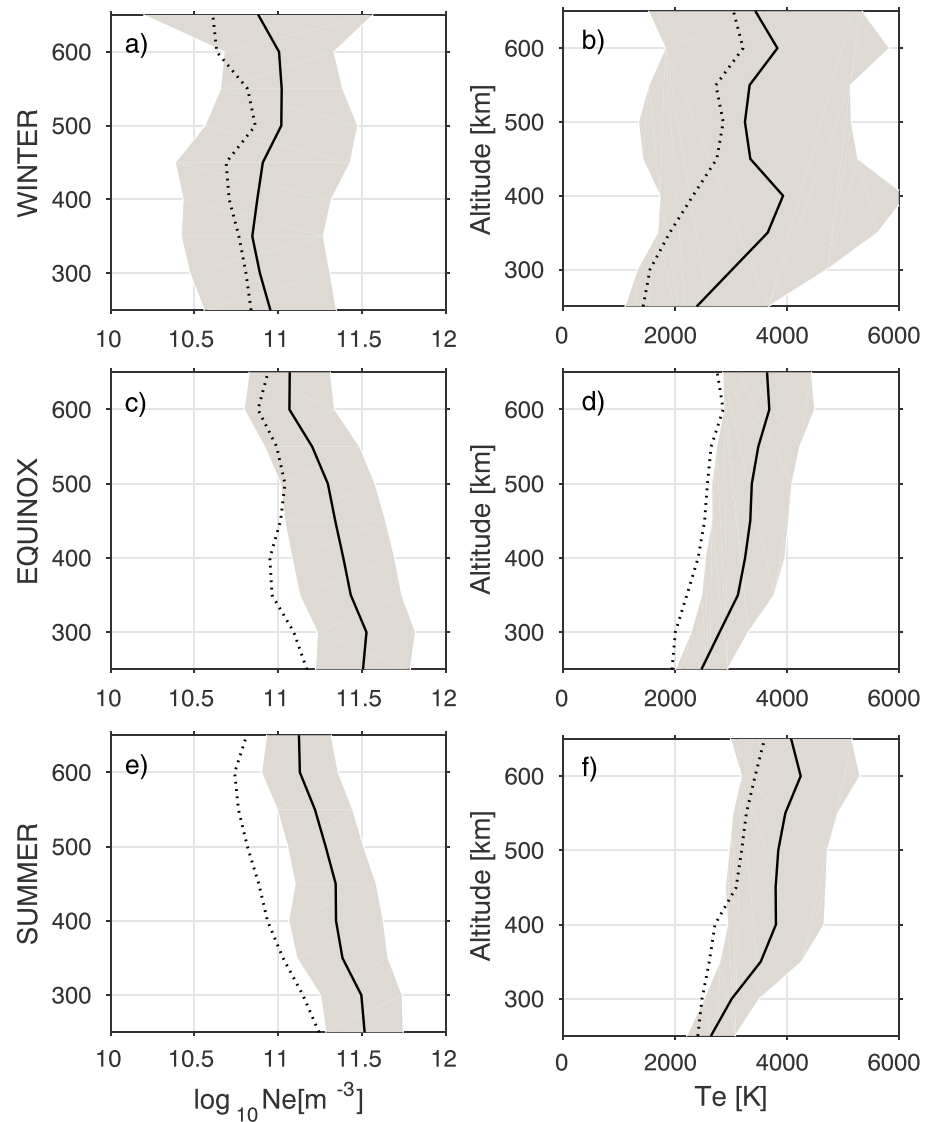


Figure 4. Distribution of electron temperature (b,d,f) and electron density (a,c,e) for winter (a,b), equinox (c,d), and summer (e,f), associated with the strong thermal component. The black line shows the strong thermal average with the gray shading marking the standard deviation of the strong thermal distribution. The dotted line shows the seasonal mean for reference. The thermal emission electron temperature is higher at solar minimum than at solar maximum. The thermal emission electron density is higher at solar maximum than at solar minimum.

The output of the model as well as the inputs are categorized in seasons of the year and solar maximum and minimum. Further analyses are done to investigate the seasonal and solar cycle variations and dependences.

3. Observations and Results

Throughout this paper, *strong thermal emission* refers to all calculated thermally excited emission intensities exceeding 1 kR. A detailed rationale for this categorization is given by Kwagala et al. (2018). Any use of terms like thermal component or thermally excited emissions will be referring to the strong thermal component.

3.1. Solar Cycle Variations

Figure 1 gives an overview of data distribution for solar maximum (red) and solar minimum (blue). Although there is more data for solar minimum (Figure 1c) than solar maximum (Figure 1a), the data are evenly distributed at all MLTs. The strong thermal component is normalized to percentage for comparison. The occurrence rate of the strong thermal component is highest at solar maximum (Figure 1b). The peak occurrence rate reaches ~40% for solar maximum (Figure 1b), whereas that for solar minimum (Figure 1d) is only ~2%.

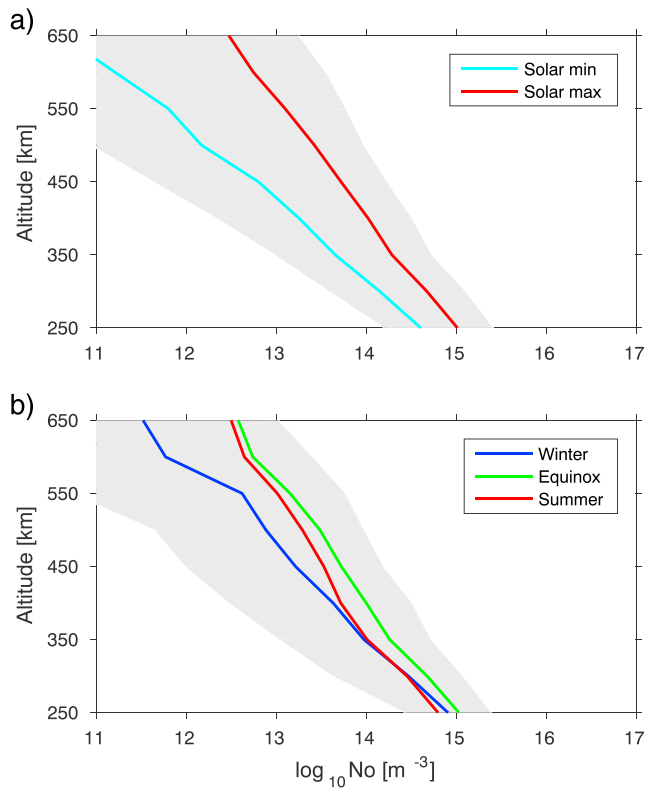


Figure 5. The NRLMSISE-00 model atomic oxygen density averaged at each altitude, for the strong thermal component. (a) Solar maximum (red) and solar minimum (cyan). (b) Winter (blue), equinox (green), and summer (red). The gray shading shows the spread of the atomic oxygen densities. The density is highest at solar maximum (a) and equinox (b) and lowest at solar minimum and winter.

Figure 1e shows the periods for solar maximum (red) and solar minimum (blue) considered for this analysis. The periods are selected with respect to the peak and minimum sunspot number (magenta line) and f10.7 radio flux (green line) for solar maximum and minimum, respectively.

Figure 2 presents the distributions for electron density (Figures 2a and 2c) and temperature (Figures 2b and 2d) associated with the strong thermal component for solar minimum (Figures 2a and 2b) and solar maximum (Figures 2c and 2d). The black line shows the strong thermal average with the gray shading showing the standard deviation of the distributions associated with the strong thermal emission. The dotted line marks the seasonal mean for reference. We refer to the difference between strong thermal average (black line) and the seasonal mean (dotted line) as the parameter enhancement (Δ). Generally, the electron temperatures and densities are enhanced for the strong thermal component, as expected. However, the electron temperature enhancement (ΔT_e) is largest at solar minimum at altitude range 250–500 km (Figure 2b).

When we compare the strong thermal associated parameters for solar minimum (Figures 2a and 2b) with those for solar maximum (Figures 2c and 2d), we find that the strong thermal component at solar minimum has higher electron temperatures than at solar maximum. Furthermore, the electron densities associated with the strong thermal component at solar maximum are generally higher than those at solar minimum. The higher background electron density at solar maximum is likely responsible for the high occurrence rate and therefore the solar cycle variations that we see.

3.2. Seasonal Variations

To investigate the seasonal variation, the data are subdivided into four seasons. Figure 3 presents an overview of the data coverage for the four seasons: winter (Figures 3a and 3b), spring (Figures 3c and 3d), summer (Figures 3e and 3f), and autumn (Figures 3g and 3h). Winter is from 20 November to 20 January. Spring is from 20 February to 20 April. Summer is from 20 May to 20 July. Autumn is from 20 August to 20 October. For all seasons, the data are evenly distributed at all MLTs. The strong thermal component has the highest occurrence around magnetic noon. The highest occurrence rate of the strong thermal component is seen in autumn and spring. Autumn shows higher occurrence rate than spring on the dayside, indicating an equinoctial asymmetry. There is no significant difference seen in the occurrence rate for summer and winter.

(Figures 3e and 3f), and autumn (Figures 3g and 3h). Winter is from 20 November to 20 January. Spring is from 20 February to 20 April. Summer is from 20 May to 20 July. Autumn is from 20 August to 20 October. For all seasons, the data are evenly distributed at all MLTs. The strong thermal component has the highest occurrence around magnetic noon. The highest occurrence rate of the strong thermal component is seen in autumn and spring. Autumn shows higher occurrence rate than spring on the dayside, indicating an equinoctial asymmetry. There is no significant difference seen in the occurrence rate for summer and winter.

Figure 4 shows the electron density and temperature distributions associated with the strong thermal component for winter (Figures 4a and 4b), equinox (Figures 4c and 4d), and summer (Figures 4e and 4f). This figure has the same format as Figure 2. Generally, the strong thermal electron densities and temperatures are enhanced as expected. The largest electron temperature enhancement (ΔT_e) is seen in winter (Figure 4 b) at 250–450 km altitude, while ΔT_e is comparable for equinox (Figure 4d) and summer (Figure 4e) throughout the altitude range of focus (250–650 km). The electron density enhancement (ΔN_e) is largest in summer throughout the altitude range of focus, however comparable with equinox in the altitude range of 250–450 km.

4. Discussion

In this study, we have estimated the intensity of thermally excited emissions using measurements of electron temperature and density from the ESR. These measurements have been described in detail in the previous section. Atomic oxygen density is another key parameter required for thermal excitation. However, we did not have any atomic oxygen density measurements and so we used modeled atomic oxygen density from the NRLMSISE-00 model (Picone et al., 2002). We will therefore start our discussion by commenting on the modeled atomic oxygen density before discussing the solar cycle and seasonal variations seen in the previous section.

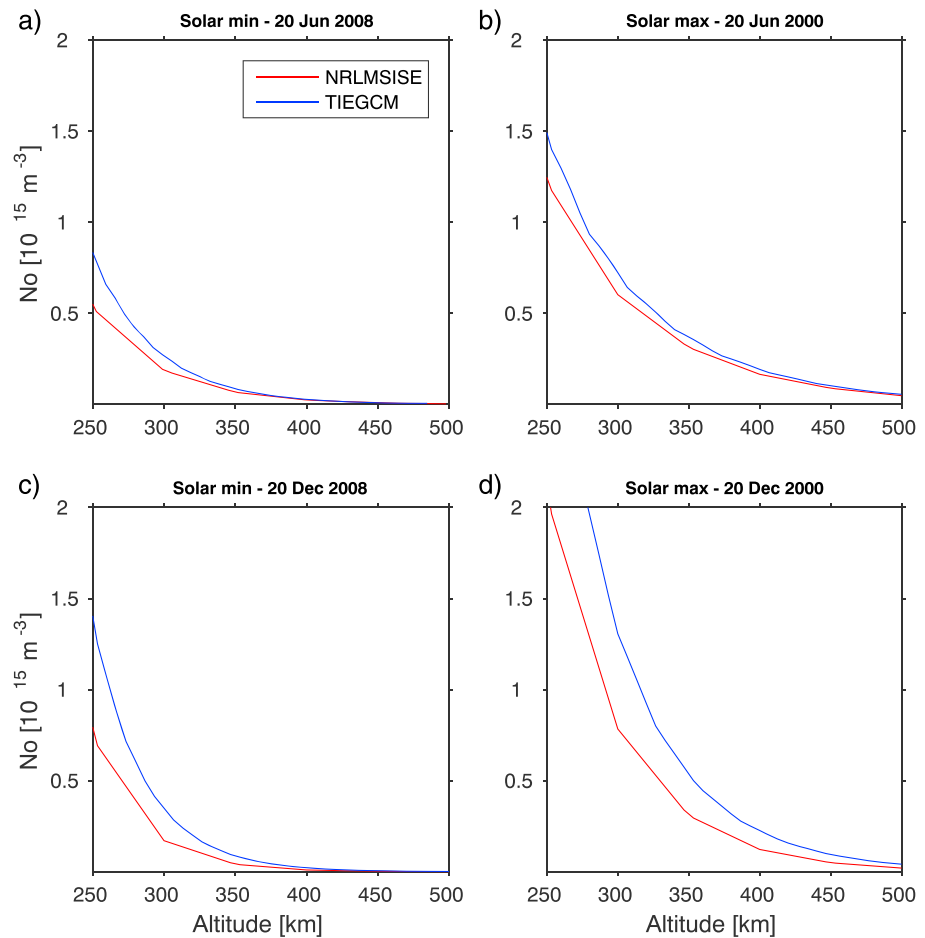


Figure 6. Comparison of atomic oxygen density modeled by NRLMSISE-00 (red) and TIE-GCM (blue), for summer (a,b) and winter (c,d) during solar minimum (a,c) and solar maximum (b,d). The TIE-GCM model gives higher atomic oxygen densities than the NRLMSISE-00 model. NRLMSISE-00 = Naval Research Laboratory Mass Spectrometer and Incoherent Scatter Radar 2000 model; TIE-GCM = Thermosphere-Ionosphere-Electrodynamics General Circulation Model.

4.1. Comment on the Modeled Atomic Oxygen Density

The atomic oxygen densities from the NRLMSISE-00 model that have been used in our study to derive the thermal component are summarized in Figure 5. The average of the modeled atomic oxygen density at each altitude associated with the strong thermal component for solar maximum (red) and solar minimum (cyan) are shown in Figure 5a. The gray shading marks the spread of the modeled atomic oxygen densities associated with the strong thermal component for the respective periods. The model shows generally higher densities for solar maximum than at solar minimum. The model shows an increase of factors ~ 6 and ~ 9 at ~ 350 and ~ 400 km, respectively, from solar minimum to solar maximum. The former and latter factors agree with Vickers et al. (2014) and Emmert and Picone (2010) who reported the same increments from estimates based on ESR measurements and satellite observations at the same altitudes, respectively.

For the seasons shown in Figure 5b, that is, winter (blue), equinox (green), and summer (red), the model shows some variations, with highest densities for equinox and lowest for winter. This is the expected seasonal variation of thermospheric density reported in literature (e.g., Vickers et al., 2013, and references therein). According to the model, there are just minor atomic oxygen density enhancements (ΔN_o) associated with the strong thermal component which show no solar cycle variations and minor seasonal variations. Therefore, the variations we see in thermal emissions are unlikely to be due to variations in atomic oxygen density but rather variations in electron density and temperature.

When we compare the atomic oxygen density from NRLMSISE-00 model with the density from the physics-based TIE-GCM model (e.g., Qian et al., 2014; Richmond et al., 1992; Roble et al., 1988), we get the

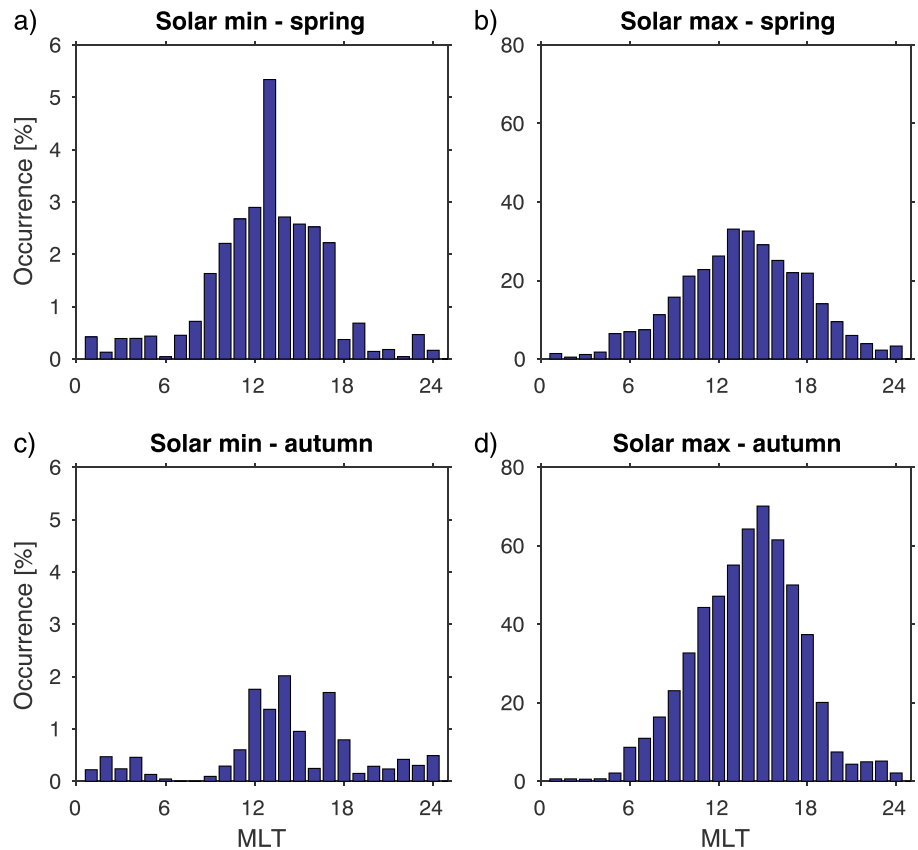


Figure 7. Equinoctial asymmetry in the occurrence of the strong thermal component. Spring (a,b) and autumn (c,d) for solar minimum (a,c) and solar maximum (b,d). The asymmetry reverses from solar minimum to solar maximum. MLT = magnetic local time.

results shown in Figure 6. Figure 6 shows the comparison between the atomic oxygen density from the two models for selected days in summer (Figures 6a and 6b) and winter (Figures 6c and 6d) for solar minimum (Figures 6a and 6c) and solar maximum (Figures 6b and 6d). Generally, the NRLMSISE-00 model produces lower atomic oxygen density than TIE-GCM. This comparison shows that the difference is biggest for winter irrespective of the solar cycle, where the TIE-GCM shows over 50% higher atomic oxygen density than the NRLMSISE-00 model that we used. Our estimates and the following discussion, therefore, are a lower limit.

4.2. Solar Cycle Variation of Thermally Excited Emissions

The occurrence rate of thermally excited emission for solar maximum and solar minimum have been presented in Figure 1. The strong thermally excited emissions occur ~20 times more frequently for solar maximum than solar minimum. The activity at the sun is highest during solar maximum (e.g., Hathaway, 2010). This implies increased solar wind-magnetosphere coupling and so higher chances of magnetosphere-ionosphere coupling via particle precipitation on the dayside. We should therefore expect the ambient electrons in the polar ionosphere to be heated more frequently via this process during solar maximum compared to solar minimum. In addition, the background electron density is generally higher for solar maximum compared to solar minimum (see Figures 2a vs. 2c). Therefore, relatively less electron temperature enhancement (ΔT_e) is required to potentially reach the thermal excitation level for solar maximum compared to solar minimum; hence, the low occurrence rate should be expected at solar minimum (see Figure 1d). In addition, the electron densities are generally low for solar minimum, hence raising the electron temperature even higher for thermal excitation to become significant. Generally, with the higher electron density background, just a small increase in electron temperature is needed, which may explain the amplified solar cycle variation.

We also note that the data from the field-aligned ESR might be biased depending on whether the field of view is inside the polar cap or not. The latitudinal location of the open/closed field boundary marks the boundary of the polar cap on the dayside (e.g., Cowley & Lockwood, 1992). On the dayside, the equatorward boundary

of the 630.0 nm auroral emission has been used to mark the open/closed field line boundary (e.g., Johnsen & Lorentzen, 2012; Johnsen et al., 2012). Johnsen and Lorentzen (2012) found seasonal variations in the latitudinal location of the open/closed boundary. They showed that during solar minimum, when the polar cap has contracted, the auroral activity is likely to move poleward of ESR beam. Therefore, thermally excited emissions could potentially be occurring but outside the ESR beam. This could potentially explain the low occurrence rate of thermal emission seen at solar minimum. However, if this was entirely responsible for the solar cycle variation we see, the thermal emission electron density and temperature at solar maximum and solar minimum would be comparable. According to Figure 2, this is not the case.

4.3. Seasonal Variation of Thermally Excited Emissions

The thermally excited emissions have been found to have the highest occurrence at equinox. There is no difference found in the occurrence rate of thermal emissions in winter and summer. This is due to the variations in electron density and electron temperature and not atomic oxygen. Other studies on other aspects like geomagnetic activity, cross-polar potential, and ionospheric conductance report similar seasonal variations (e.g., Cliver et al., 2000, 2002; Cnossen et al., 2012; Russell & McPherron, 1973). These attributed the seasonal variations to magnetic reconnection processes (e.g., Cnossen et al., 2012), and an equinoctial effect which makes the southward B_z coupling less effective at the solstices (e.g., Cliver et al., 2000).

Kervalishvili and Lühr (2013) reported seasonal variations of the electron temperature similar to ours, from a statistical study of thermospheric mass density enhancement. The authors found the electron temperature enhancement largest in winter, just as the electron temperature associated with the strong thermal component in the current study. Such thermospheric mass density enhancement are believed to be a result of neutral upwelling (e.g., Lühr et al., 2004). Earlier studies have reported a possible coincident occurrence of thermally excited emissions and neutral upwelling (e.g., Kwagala et al., 2017). Both neutral upwelling and thermally excited emissions are believed to be driven by the dayside magnetic reconnection and associated with soft electron precipitation and electron temperature enhancements in the cusp ionosphere, with the former associated with joule heating and the latter associated with direct electron heating by precipitating soft electrons (e.g., Carlson et al., 2013; Kwagala et al., 2017, 2018; Lühr et al., 2004; Prölss, 2008; Sadler et al., 2012; Zhang et al., 2012). It indicates that the two phenomena could be occurring during the same connected chain of processes in the cusp.

The background electron temperature and density include among others the contribution from the solar EUV radiation and precipitation. During winter at Svalbard, the sun is below the horizon (zenith angle $>90^\circ$), therefore the direct solar EUV radiation contribution is reduced which could explain the lower electron density and temperature. Since the strong thermal component occurs on the dayside, the enhancements seen in winter could mainly be a result of the precipitation from the dayside magnetopause reconnection (see Figures 4a and 4b). Due to the already existing relatively low electron densities, large electron temperature enhancements are necessary for the thermally excited emissions to occur, which could explain the few occurrences in winter. We are also of the view that solar EUV radiation heats both ions and electrons at the same rate, and heated electrons will effectively cool via the ordinary mechanism of collision with the ions. Thus, thermal balance will to a large extent be maintained. Therefore, for summer, only when the precipitating electrons from the dayside reconnection heat the ionospheric electrons at a faster rate than the ambient ion-electron collision will it give rise to the strong thermal emissions. For this reason, the strong thermal emissions should not be frequent during summer.

When we analyze the potential bias in the ESR data due to its location with respect to the polar cap, the size of the polar cap has been reported to possibly vary in response to variations in solar wind-magnetosphere coupling (Cnossen & Richmond, 2012). Since this coupling is highest at equinox, we would expect the polar cap to be in the ESR 42-m field of view more frequently. To back this up, the electron temperature (see Figures 4d and 4f) and density (see Figures 4c and 4e) in equinox and summer are comparable, when the contribution of solar EUV radiation is expected to be relatively the same on the dayside (sun above horizon). This could imply that the higher occurrence rate of thermal emissions at equinox is biased by the potential higher frequency of the polar cap in the field of view of the ESR 42 m beam.

Furthermore, the thermal component does not occur at the same rate on the dayside for spring and autumn. The equinoctial asymmetry (see Figures 3d vs. 3h) observed in the occurrence rates of thermally excited emissions could be related to the R-M effect (Russell & McPherron, 1973). The R-M effect is a seasonal and diurnal variation in the Earth's dipole axis with respect to the Parker spiral interplanetary magnetic field, which leads

to periodic variations in solar wind-magnetosphere coupling. Geomagnetic activity is predicted to maximize near equinoxes, near 23 UT in spring and 11 UT in autumn. Since the MLT of Svalbard is \sim UT + 3, the R-M effect predicts peak geomagnetic activity on the dayside in autumn and on the nightside in spring. This is exactly the variation that is observed in the thermal emissions. Based on this argument, we predict an opposite equinoctial asymmetry in thermal emissions in the American sector. This argument was first presented by Aruliah et al. (1996), who found an equinoctial asymmetry in thermospheric winds observed in Kiruna, in the same longitude sector as Svalbard. Their observations were from the nightside, and therefore the equinoctial asymmetry was opposite of what we find here. Our results (see Figure 7) show that the equinoctial asymmetry reverses with the solar cycle. Aruliah et al. (1996) attributed the reversal of the asymmetry with the solar cycle to the location of the observation site with respect to the auroral oval which is consistent with our results.

5. Summary and Conclusion

We have made the first statistical analysis of the seasonal and solar cycle variations of the occurrence of thermally excited emissions in the polar ionosphere. The thermal emissions have been estimated from ESR measurements of electron density and temperature for the period 2000–2015. Our key findings include the following:

- The thermally excited emission mainly occurs on the dayside and maximizes around magnetic noon, irrespective of the season or solar cycle period.
- The occurrence of thermally excited emissions maximizes at solar maximum, occurring \sim 20 times more frequent than at solar minimum.
- The occurrence of thermally excited emissions varies with season and maximizes at equinox.
- There is an equinoctial asymmetry in the occurrence rate of the strong thermal emissions that is attributed to the R-M effect.
- Generally, the electron temperature, electron density, and atomic oxygen density associated with the strong thermal component are values above average. The enhancement changes with solar cycle and season.
 - a. The electron temperature enhancement is largest at solar minimum and winter.
 - b. The electron density enhancement is largest at solar maximum.

In conclusion, thermal excitation can be an important phenomenon in the polar ionosphere particularly on the dayside. Just as other aspects like geomagnetic activity, the occurrence of strong thermally excited emissions has similar seasonal and solar cycle variations. The equinoctial asymmetry attributed to variations in the solar wind-magnetosphere coupling arising from the R-M effect suggests solar wind-magnetosphere-ionosphere coupling as the dominant controlling process of the strong thermal component. The direct connection or role of thermal excitation in the polar ionosphere during phenomena or features like neutral upwelling, cusp aurora, and poleward moving auroral forms, which occur during intense MI coupling, is yet to be investigated. Finally, we strongly recommend that thermal excitation is taken into consideration whenever the 630.0 nm emission line in the polar ionosphere is used in any analysis or study.

References

- Aruliah, A. L., Farmer, A. D., Fuller-Rowell, T. J., Wild, M. N., Hapgood, M., & Rees, D. (1996). An equinoctial asymmetry in the high-latitude thermosphere and ionosphere. *Journal of Geophysical Research*, *101*(A7), 15,713–15,722. <https://doi.org/10.1029/95JA01102>
- Aruliah, A. L., Schoendorf, J., Aylward, A. D., & Wild, M. N. (1997). Modeling the high-latitude equinoctial asymmetry. *Journal of Geophysical Research*, *102*(A12), 27,207–27,216. <https://doi.org/10.1029/97JA01991>
- Carlson, H. C. (1996). Incoherent scatter radar mapping of polar electrodynamicity. *Journal of Atmospheric and Terrestrial Physics*, *58*(1), 37–56. [https://doi.org/10.1016/0021-9169\(95\)00018-6](https://doi.org/10.1016/0021-9169(95)00018-6)
- Carlson, H. C., Oksavik, K., & Moen, J. I. (2013). Thermally excited 630.0 nm O(1D) emission in the cusp: A frequent high-altitude transient signature. *Journal of Geophysical Research: Space Physics*, *118*, 5842–5852. <https://doi.org/10.1002/jgra.50516>
- Cliver, E. W., Kamide, Y., & Ling, A. G. (2000). Mountains versus valleys: Semiannual variation of geomagnetic activity. *Journal of Geophysical Research*, *105*(A2), 2413–2424. <https://doi.org/10.1029/1999JA900439>
- Cliver, E., Kamide, Y., & Ling, A. (2002). The semiannual variation of geomagnetic activity: Phases and profiles for 130 years of aa data. *Journal of Atmospheric and Solar-Terrestrial Physics*, *64*(1), 47–53. [https://doi.org/10.1016/S1364-6826\(01\)00093-1](https://doi.org/10.1016/S1364-6826(01)00093-1)
- Cnossen, I., & Richmond, A. D. (2012). How changes in the tilt angle of the geomagnetic dipole affect the coupled magnetosphere-ionosphere-thermosphere system. *Journal of Geophysical Research*, *117*, A10317. <https://doi.org/10.1029/2012JA018056>
- Cnossen, I., Wiltberger, M., & Ouellette, J. E. (2012). The effects of seasonal and diurnal variations in the Earth's magnetic dipole orientation on solar wind-magnetosphere-ionosphere coupling. *Journal of Geophysical Research*, *117*, A11211. <https://doi.org/10.1029/2012JA017825>
- Cowley, S. W. H., & Lockwood, M. (1992). Excitation and decay of solar wind-driven flows in the magnetosphere-ionosphere system. *Annales Geophysicae*, *10*, 103–115.
- Dickinson, R. E., Ridley, E. C., & Roble, R. G. (1981). A three-dimensional general circulation model of the thermosphere. *Journal of Geophysical Research*, *86*(A3), 1499–1512. <https://doi.org/10.1029/JA086iA03p01499>

Acknowledgments

The EISCAT data were accessed from <https://www.eiscat.se> and processed using GUIDAP. EISCAT is an international association supported by research organizations in China (CRIRP), Finland (SA), Japan (NIPR and STEL), Norway (NFR), Sweden (VR), and the United Kingdom (NERC). The interplanetary magnetic field and solar wind data were provided by the NASA OMNIWeb service (<https://omniweb.gsfc.nasa.gov/>). The NRLMSISE-00 Atmospheric model was accessed from <https://ccmc.gsfc.nasa.gov/modelweb/models/nrlmsise00.php>. Simulation results have been provided by the Community Coordinated Modeling Center at Goddard Space Flight Center through their public Runs on Request system (<http://ccmc.gsfc.nasa.gov/>). The TIE-GCM Model was developed by the R. G. Roble et al. at the High Altitude Observatory, National Center for Atmospheric Research (HAO/NCAR). The TIE-GCM is an open-source community model available at the HAO/NCAR web site. This project has been funded by the Norwegian Research Council under the contract 223252. Kjellmar Oksavik was also grateful for being selected as the 2017–2018 Fulbright Arctic Chair, and his sabbatical at Virginia Tech was sponsored by the U.S.-Norway Fulbright Foundation for Educational Exchange.

- Doering, J., & Gulcicek, E. (1989). Absolute differential and integral electron excitation cross sections for atomic oxygen 7. The $3^3P \rightarrow 1^1D$ and $3^3P \rightarrow 1^1S$ transitions from 4.0 to 30 eV. *Journal of Geophysical Research*, *94*, 1541–1546. <https://doi.org/10.1029/JA094iA02p01541>
- Emmert, J. T., & Picone, J. M. (2010). Climatology of globally averaged thermospheric mass density. *Journal of Geophysical Research*, *115*, A09326. <https://doi.org/10.1029/2010JA015298>
- Hathaway, D. H. (2010). The solar cycle. *Living Reviews in Solar Physics*, *7*(1), 1. <https://doi.org/10.12942/lrsp-2010-1>
- Henry, R., Burke, P., & Sinfailam, A.-L. (1969). Scattering of electrons by C, N, O, N⁺, O⁺, and O⁺⁺. *Physical Review*, *178*, 218–225. <https://doi.org/10.1103/PhysRev.178.218>
- Johnsen, M. G., & Lorentzen, D. A. (2012). A statistical analysis of the optical dayside open/closed field line boundary. *Journal of Geophysical Research*, *117*, A02218. <https://doi.org/10.1029/2011JA016984>
- Johnsen, M. G., Lorentzen, D. A., Holmes, J. M., & Løvhaug, U. P. (2012). A model based method for obtaining the open/closed field line boundary from the cusp auroral 6300 Å [O] red line. *Journal of Geophysical Research*, *117*, A03319. <https://doi.org/10.1029/2011JA016980>
- Kervalishvili, G. N., & Lühr, H. (2013). The relationship of thermospheric density anomaly with electron temperature, small-scale FAC, and ion up-flow in the cusp region, as observed by CHAMP and DMSP satellites. *Annales Geophysicae*, *31*, 541–554. <https://doi.org/10.5194/angeo-31-541-2013>
- Kozyra, J. U., Valladares, C. E., Carlson, H. C., Buonsanto, M. J., & Slater, D. W. (1990). A theoretical study of the seasonal and solar cycle variations of stable aurora red arcs. *Journal of Geophysical Research*, *95*(A8), 12,219–12,234. <https://doi.org/10.1029/JA095iA08p12219>
- Kwagala, N. K., Oksavik, K., Lorentzen, D. A., & Johnsen, M. G. (2017). On the contribution of thermal excitation to the total 630.0 nm emissions in the northern cusp ionosphere. *Journal of Geophysical Research: Space Physics*, *122*, 1234–1245. <https://doi.org/10.1002/2016JA023366>
- Kwagala, N. K., Oksavik, K., Lorentzen, D. A., & Johnsen, M. G. (2018). How often do thermally excited 630.0 nm emissions occur in the polar ionosphere? *Journal of Geophysical Research: Space Physics*, *123*, 698–710. <https://doi.org/10.1002/2017JA024744>
- Lan, V. K., Feautrier, N., Dourneuf, M. L., & Regemorter, H. V. (1972). Cross sections calculations for electron oxygen scattering using the polarized orbital close coupling theory. *Journal of Physics B: Atomic and Molecular Physics*, *5*(8), 1506–1516.
- Laundal, K. M., & Richmond, A. D. (2017). Magnetic coordinate systems. *Space Science Reviews*, *206*(1), 27–59. <https://doi.org/10.1007/s11214-016-0275-y>
- Lockwood, M., Carlson, H. C., & Sandholt, P. E. (1993). Implications of the altitude of transient 630-nm dayside auroral emissions. *Journal of Geophysical Research*, *98*(A9), 15,571–15,587. <https://doi.org/10.1029/93JA00811>
- Lühr, H., Rother, M., Köhler, W., Ritter, P., & Grunwaldt, L. (2004). Thermospheric up-welling in the cusp region: Evidence from CHAMP observations. *Geophysical Research Letters*, *31*, L06805. <https://doi.org/10.1029/2003GL019314>
- Mantas, G. P., & Carlson, H. C. (1991). Reexamination of the O($3^3P \rightarrow 1^1D$) excitation rate by thermal electron impact. *Geophysical Research Letters*, *18*(2), 159–162. <https://doi.org/10.1029/91GL00019>
- Picone, J. M., Hedin, A. E., Drob, D. P., & Aikin, A. C. (2002). NRLMSISE-00 empirical model of the atmosphere: Statistical comparisons and scientific issues. *Journal of Geophysical Research*, *107*(A12), 1468. <https://doi.org/10.1029/2002JA009430>
- Pröls, G. W. (2008). Perturbations of the upper atmosphere in the cleft region. *Journal of Atmospheric and Solar-Terrestrial Physics*, *70*, 2374–2380. <https://doi.org/10.1016/j.jastp.2008.06.017>
- Qian, L., Burns, A. G., Emery, B. A., Lu, G., Maute, A., et al. (2014). *The NCAR TIE-GCM*. Chichester, UK: John Wiley and Sons, Ltd. <https://doi.org/10.1002/9781118704417.ch7>
- Qian, L., Solomon, S. C., & Kane, T. J. (2009). Seasonal variation of thermospheric density and composition. *Journal of Geophysical Research*, *114*, A01312. <https://doi.org/10.1029/2008JA013643>
- Richmond, A. D. (1995). Ionospheric electrodynamics using magnetic apex coordinates. *Journal of Geomagnetism and Geoelectricity*, *47*(2), 191–212. <https://doi.org/10.5636/jgg.47.191>
- Richmond, A. D., Ridley, E. C., & Roble, R. G. (1992). A thermosphere/ionosphere general circulation model with coupled electrodynamics. *Geophysical Research Letters*, *19*(6), 601–604. <https://doi.org/10.1029/92GL00401>
- Roble, R. G., Dickinson, R. E., & Ridley, E. C. (1977). Seasonal and solar cycle variations of the zonal mean circulation in the thermosphere. *Journal of Geophysical Research*, *82*(35), 5493–5504. <https://doi.org/10.1029/JA082i035p05493>
- Roble, R. G., Dickinson, R. E., & Ridley, E. C. (1982). Global circulation and temperature structure of thermosphere with high-latitude plasma convection. *Journal of Geophysical Research*, *87*(A3), 1599–1614. <https://doi.org/10.1029/JA087iA03p01599>
- Roble, R. G., Ridley, E. C., Richmond, A. D., & Dickinson, R. E. (1988). A coupled thermosphere/ionosphere general circulation model. *Geophysical Research Letters*, *15*(12), 1325–1328. <https://doi.org/10.1029/GL015i012p01325>
- Russell, C. T., & McPherron, R. L. (1973). Semiannual variation of geomagnetic activity. *Journal of Geophysical Research*, *78*(1), 92–108. <https://doi.org/10.1029/JA078i001p00092>
- Sadler, F. B., Lessard, M., Lund, E., Otto, A., & LÄhr, H. (2012). Auroral precipitation/ion upwelling as a driver of neutral density enhancement in the cusp. *Journal of Atmospheric and Solar-Terrestrial Physics*, *87–88*, 82–90. <https://doi.org/10.1016/j.jastp.2012.03.003>
- Thomas, L. D., & Nesbet, R. K. (1975). Low-energy electron scattering by atomic oxygen. *Physical Review A*, *11*, 170–173. <https://doi.org/10.1103/PhysRevA.11.170>
- Vickers, H., Kosch, M. J., Sutton, E., Bjoland, L., Ogawa, Y., & La Hoz, C. (2014). A solar cycle of upper thermosphere density observations from the EISCAT Svalbard Radar. *Journal of Geophysical Research: Space Physics*, *119*, 6833–6845. <https://doi.org/10.1002/2014JA019885>
- Vickers, H., Kosch, M. J., Sutton, E., Ogawa, Y., & La Hoz, C. (2013). Thermospheric atomic oxygen density estimates using the EISCAT Svalbard Radar. *Journal of Geophysical Research: Space Physics*, *118*, 1319–1330. <https://doi.org/10.1002/jgra.50169>
- Wannberg, G., Wolf, I., Vanhainen, L.-G., Koskenniemi, K., Röttger, J., Postila, M., et al. (1997). The EISCAT Svalbard radar: A case study in modern incoherent scatter radar system design. *Radio Science*, *32*(6), 2283–2307. <https://doi.org/10.1029/97RS01803>
- Zhang, B., Lotko, W., Brambles, O., Wiltberger, M., Wang, W., Schmitt, P., & Lyon, J. (2012). Enhancement of thermospheric mass density by soft electron precipitation. *Geophysical Research Letters*, *39*, L20102. <https://doi.org/10.1029/2012GL053519>
- Zhao, H., & Zong, Q.-G. (2012). Seasonal and diurnal variation of geomagnetic activity: Russell-McPherron effect during different IMF polarity and/or extreme solar wind conditions. *Journal of Geophysical Research*, *117*, A11222. <https://doi.org/10.1029/2012JA017845>